

# Deconvolution of fission-track length distributions and its application to dating and separating pre- and post-depositional components Age distribution of horizontal fission tracks

5 Peter Klint Jensen<sup>1</sup>, Kirsten Hansen<sup>2</sup>

<sup>1</sup>DTU Civil Engineering, Technical University of Denmark, Kgs. Lyngby, DK-2800, Denmark

<sup>2</sup>Natural History Museum of Denmark, University of Copenhagen, Copenhagen, DK-1350, Denmark

Correspondence to: Peter Klint Jensen (pklje@byg.dtu.dk)

**Abstract.** To enable the separation between pre- and post-depositional components of the length distribution of (partially annealed) horizontal confined fission tracks it is corrected by deconvolution. Equations for the distribution of age versus length of partially annealed horizontal fission tracks in apatite is presented. Probabilistic least-squares inversion corrects natural track length histograms for observational biases considering the variance of data, modelization, and prior information. The corrected histogram is validated by its variance-covariance matrix. It is considered that horizontal track data can be with or without measurements of angles to the c-axis. In the last case, 3D-histograms are introduced as an alternative to histograms of c-axis projected track lengths. Thermal history modeling of samples is not necessary for the calculation of track age distributions of corrected tracks-ealeulation. In an example the age equations are applied to apatites with pre-depositional (inherited) tracks, to extract the post-depositional track length histogram. Fission tracks generated before deposition in detrital apatite crystals are mixed with post-depositional tracks. This complicates the calculation of the post-sedimentary thermal history as the grains have experienced different thermal histories until deposition. Thereafter the grains share a common thermal history. Therefore  
20 the extracted post-depositional histogram without inherited tracks may be used for thermal history calculation.

## 1 Overview of the formation of fission tracks

Fission of U-238 in apatite, titanitesphene, and zircon create tracks in the crystal lattice. Track density is reduced as a function of temperature and time as tracks anneal and shorten due to atom diffusivity (Li et al., 2011; Fleisher et al., 1975; Afra et al., 2011). The ongoing track generation through time and simultaneous annealing is used to derive the thermal history of the  
25 sample. Bertagnolli et al. (1983) derived the differential equation describing the track length distribution within a mineral due to annealing through time. The surface density of tracks is also described. Forward calculation examples are given by Bertagnolli et al. (1983). On this basis, Keil et al. (1987) developed an inversion procedure, where the temperature history is derived from either the length distribution of tracks within the crystal or from the length distribution of projected tracks intersecting the surface. The calculation procedure is direct and without the use of a Monte Carlo type optimization. The time  
30 of track generation can be derived from the observed track length distribution independent of any annealing modellaw (Keil et al., 1987):

$$\tau(\lambda_0) = \frac{1}{\varepsilon} \int_1^{\lambda_0} n(\lambda) d\lambda, \quad (1)$$

where  $\lambda_0$  is the present track normalized length,  $\varepsilon$  is the fission-track production rate,  $n(\lambda)$  is the measured number of fission tracks of length  $\lambda$  produced per volume. Equation (1) is understood as follows: The annealing properties of the mineral affect the final apparent age as well as the expected age of the oldest randomly oriented unetched track. However, the expected age of this track can be determined by counting the number of all tracks in a volume and divide by the track generation rate. In the simplified case of no spread of track lengths, the expected age of any given track is calculated by counting the number of shorter tracks plus one. This age is determined without the use of an annealing model. The unetched tracks are not routinely measured. Etched confined horizontal tracks are measured instead. This manuscript explains how they can be used together with the surface track density to separate pre- and post-depositional components.

The temperature history is derived from the distribution of projected tracks together with an annealing model. Keil et al. (1987) showed, by a synthetic example for projected tracks, that the thermal history can be calculated numerically stepwise backward in time starting with the present temperature. The large uncertainties of projection of tracks mean that the approach by Keil et al. (1987) is dubious. The selection of horizontal, confined tracks ~~are~~ recommended instead (Laslett et al., 1984), that is “tracks identified by the constancy of focus over their entire length and strong reflection in incident illumination” (Gleadow et al., 1986b; Gleadow et al., 2019). The model by Keil et al. (1987) does not include blurring of track length histograms caused by the initial distribution of fission fragment energy (Jungerman and Wright, 1949), annealing and etching anisotropy, mineral composition, the uncertainty of measurement (Ketcham, 2003), and track selection biases Jensen et al. (1992). Proportionality of the number of tracks in a track length histogram column and time assumed by Keil et al. (1987) is disturbed by the blurring. Jensen et al. (1992; 1993) extended Eq. (1) to confined horizontal tracks instead of projected tracks. ~~Belton and Raab (2010) also used a backward-cumulative method to estimate the track ages. Donelick (1988) introduced a fission track inversion procedure based on principles like that of Jensen et al. (1992) and the present paper.~~

Three major biases appear to be important when deriving the equation for track age: 1) Surface track density bias reflecting the likelihood of a track to be exposed to etching on the surface. We use an exponential approximation to surface track density versus mean track length for induced tracks annealed in the laboratory (Green, 1988). 2) Track length bias due to the likelihood of a track being exposed to etching through fractures and tracks cutting the etched surface. We assume it to be proportional to the track length. 3) Selection bias due to the likelihood of an etched track being accepted as horizontal. We assume that tracks within a given angle from the horizontal are counted. The alternative that all tracks in focus are accepted is discussed in Appendix DC. Besides biases, there is a range of effects contributing to large observational deviations of track lengths as has been documented in interlaboratory comparisons (Ketcham et al., 2009). The effects are caused by a) fluid filling track tips, b) poorly chosen track tips, c) analyst inexperience, personal etching and observational practice, and sampling statistics. Variation of the number of tracks in a given length interval is dependent on the spontaneous character of fission. The

65 disordering of the unique relationship between track length and time caused by various biases and variances is essentially  
restored by deconvolution of natural track length histograms (Jensen et al., 1992). Deconvolution is performed by  
mathematically simulated annealing (Kirkpatrick et al., 1983) and with the use of filters based on annealing of induced tracks  
in the laboratory. Jensen et al. (1992; 1993) and Jensen and Hansen (2018) used that the corrected track ages can be derived  
separately from the thermal history as shown by Keil et al. (1987). The columns of the deconvolved track length histogram are  
70 then converted to equivalent time intervals. The track ages are obtained by backward cumulation from long tracks toward short  
tracks. We are not assigning an age to the bins of observed fission-track length histograms. Ages are assigned to the bins of  
the deconvolved (corrected) track length histograms which can then be used to age date thermal events. The procedure of  
deconvolution procedure described in Jensen et al. (1992) is for measurements where the c-axis angle is not measured. When  
they are available it is the practice to project the tracks on the crystal c-axis following the procedure described by Donelick et  
75 al. (1999). As an alternative, the inversion method presented here uses 3D-histograms. Age-track-length relations for corrected  
tracks are given explicitly in contrast to the indirectly embedded relations in the computer programesprograms by Green et al.  
(1989), Lutz and Omar (1991), Ketcham (2005), and Gallagher (2012). Our age calculations are calibrated without sample  
temperature history modeling. The inversion procedure presented here is based on least-squares probabilistic inverse theory  
(Tarantola, 2005). The method is computational fast.

## 80 2 Summary of age and temperature calculation

Before entering the mathematics of age calculation, a recipe for age dating of an uplift event is given including temperature  
calculation. First, an idealized model is considered with tracks generated continuously (not spontaneously), no length spreading  
during annealing, no etching, and no errors of measurements:

- 85 1. Construct a track length density histogram (numbers/volume) of the randomly oriented unetched tracks.
2. Convert the track length histogram into a histogram of time intervals by dividing the number of tracks in each column  
by the rate of track generation. Each column of this histogram represents the time it takes to generate the tracks  
belonging to the columns.
3. Cumulate the time intervals from the youngest (longest tracks) to the oldest (shortest tracks) to obtain a histogram of  
track ages.
- 90 4. If the uplift is sufficiently pronounced a statistically significant break is visible in the age histogram. The event is  
hereby age-dated.
5. The age of the event can be used to extract the pre-event track histogram from the left part (shortest tracks) of the  
cumulated ages and the post-event histogram from the right part (longest tracks). To this point, there has been no  
need for a track annealing model.

95 6. The post-event temperature histories can now be calculated separately which is useful if the pre-event tracks are of mixed origins. The temperature is calculated for each column of the time interval histogram, as explained in Jensen et al. (1992).

100 In practice, however, confined horizontal etched track length histograms are used together with the surface track density, for age dating and calculation of the history of temperature. Tracks are produced spontaneously, their lengths are spread during annealing, observations are biased, and measurements are uncertain. The recipe then sounds:

1. Construct a track length histogram of the observed confined horizontal etched tracks.
2. Remove the spreading of track lengths by deconvolution (deblurring) of the observed histogram.
- 105 3. Use the deconvolved histogram for age dating and calculation of the history of temperature following the recipe from point 2. for the idealized tracks.

110 The recipes are based on the development by Bertagnolli (1983), Keil et al. (1987), and Jensen et al. (1992). See also Donelick (1988) for a similar development. The procedure for calculating the temperature history based on the deconvolved track length histogram was presented by Jensen et al. (1992). At that time, deconvolution was performed by trial and error. Mathematically simulated annealing was later applied instead (Jensen and Hansen, 2018). Age dating and identification of inherited tracks using Tarantola inversion are presented in the next sections. The calculations are direct with no use of Monte Carlo simulations. Readers unfamiliar with the technique of deconvolution may benefit from reading Appendix A before entering the Tarantola inversion technique.

### 115 32 Correcting for biases of track length histograms by deconvolution~~Equation for the age distribution~~

Consider a mineral as apatite and a time interval  $\Delta t^i$  in which randomly oriented fission tracks are generated with the initial track length  $L_0$ . The number of tracks per unit volume generated in the time interval is proportional to the fission decay frequency  $\lambda_f$ , the uranium U-238 concentration  $c$ , and the length of the time interval  $\Delta t^i$ :

$$n^i = \lambda_f c \Delta t^i \text{ for } i = 1 \dots N. \quad (2)$$

120  $N$  is the number of time intervals. The exponential decay of U-238 nuclei is ignored, to begin with. A track is generated for each fission; therefore,  $n^i$  is also the number of initially randomly oriented tracks per unit volume. The track length histogram of the randomly oriented tracks per unit volume generated in a single time interval  $\Delta t^i$  is initially

$$\mathbf{n}^i = (n_1^i \dots n_j^i \dots n_M^i)^T. \quad (3)$$

125 Vectors are bold and the transpose  $^T$  transforms rows into columns.  $M$  is the number of track length bins. The tracks are gradually annealed from the initial length by temperature and time leading to shorter tracks with the mean track length  $L^i$  (Fig.

1). The tracks generated in the time interval  $\Delta t^i$  are after partial annealing distributed into various track length columns. At present, after partial annealing, the track length histogram is

$$\mathbf{v}^i = (v_1^i \dots v_j^i \dots v_M^i)^T. \quad (4)$$

For the tracks that are not annealed below the detection limit the number of tracks per unit volume  $v^i$  (not bold) is equal to the number of fissions in the time interval that is

$$v^i = \sum_{j=1}^M v_j^i = n^i = \lambda_f c \Delta t^i. \quad (5)$$

The surface track density is initially  $\sigma_0^i$  and at present  $\sigma^i$ , Fig. 1.

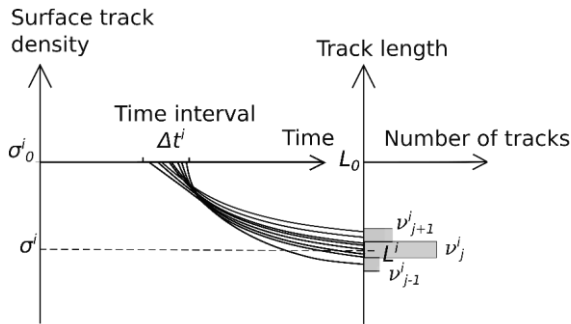


Figure 1: In the time interval  $\Delta t^i$ , several tracks are spontaneously generated with the initial mean track length  $L_0$  and surface density  $\sigma_0^i$ . During anisotropic annealing over time, the initial length is reduced along the curved path and spread around the present mean length  $L^i$ . Tracks from neighborneighbouring time intervals are similarly spread and consequently mixed with tracks from the time interval  $\Delta t^i$ .

A fraction of the randomly oriented tracks  $\mathbf{v}^i$  cut other tracks connected to the surface providing paths for etchants making them observable in the light microscope. The near-horizontal tracks are selected for length measurements. The track length histogram of the observed near-horizontal tracks generated in the time interval  $\Delta t^i$  is

$$\mathbf{h}^i = (h_1^i \dots h_j^i \dots h_M^i)^T. \quad (6)$$

$\mathbf{h}^i$  is expected to be linearly dependent on the randomly orientated unexposed tracks  $\mathbf{v}^i$  which means that the histogram  $\mathbf{h}^i$  is derived by multiplying the histogram  $\mathbf{v}^i$  by a set of constants  $Kk_1^i, \dots, Kk_M^i$ :

$$\mathbf{h}^i = K(k_1^i v_1^i \dots k_j^i v_j^i \dots k_M^i v_M^i)^T, \quad (7)$$

where  $K$  is a proportionality constant. Equation (7) relates the partly annealed randomly oriented unetched tracks to the observed horizontal tracks. The  $j$ 'th elements of  $\mathbf{h}^i$  is

$$h_j^i = K k_j^i v_j^i. \quad (8)$$

The number of observable tracks generated in the time interval  $\Delta t^i$  is

$$h^i = \sum_{j=1}^M h_j^i = K \sum_{j=1}^M k_j^i v_j^i. \quad (9)$$

Horizontal confined tracks of large area (the product of etched length and width) are likely to be etched  
~~It is expected that long tracks are more likely to be etched and observed than short tracks when using the angle selection criteria~~  
(Ketcham, 2019). This means that the proportionality constants are as follows:

$$k_j^i = \frac{L_j^i}{L_0}, \quad (10)$$

where  $L_j^i$  is the track length of the partially annealed track. The relation between the randomly oriented tracks to the number of observable tracks is then

$$h^i = \frac{K}{L_0} \sum_{j=1}^M (L_j^i v_j^i). \quad (11)$$

Equation (8) and Eq. (10) lead to:

$$\frac{L_0}{K L_j^i} h_j^i = v_j^i. \quad (12)$$

Summation on both sides of the equation leads to

$$\frac{L_0}{K} \sum_{j=1}^M \frac{h_j^i}{L_j^i} = \sum_{j=1}^M v_j^i = v^i = n^i = \lambda_f c \Delta t^i, \quad (13)$$

which means that

$$\Delta t^i = \frac{L_0}{K \lambda_f c} \sum_{j=1}^M \frac{h_j^i}{L_j^i}. \quad (14)$$

It is expected that the shape and mean track length of the histogram  $\mathbf{h}^i$  of observable tracks with origin in the time interval  $\Delta t^i$  can be reproduced in a laboratory annealing experiment:

$$\mathbf{h}^i = \mathcal{H}^i \mathbf{g}^i, \quad (15)$$

where  $\mathcal{H}^i$  is a proportionality constant.  $\mathbf{g}^i$  is a track length distribution histogram derived from annealing in the laboratory, or an interpolation thereof:

$$\mathbf{g}^i = (g_1^i, g_2^i, \dots, g_j^i, \dots, g_M^i)^T. \quad (16)$$

$\mathbf{g}^i$  and  $\mathbf{h}^i$  have identical mean track lengths.

$$h^i = \sum_{j=1}^M \mathbf{h}^i = \sum_{j=1}^M \mathcal{H}^i g_j^i = \mathcal{H}^i \sum_{j=1}^M g_j^i = \mathcal{H}^i, \quad (17)$$

because  $\mathbf{g}^i$  is normalized for all  $i$ :

$$\sum_{j=1}^M g_j^i = 1 \quad (18)$$

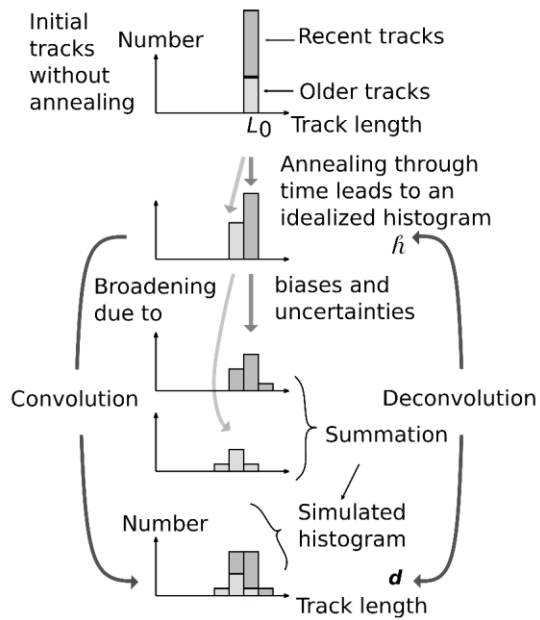
The natural observed histogram is the sum over all the histograms  $\mathbf{h}^i$ , each of which linked to time interval  $i$ :

$$\mathbf{d} = \sum_{i=1}^N \mathbf{h}^i, \quad (19)$$

and with Eq. (15)

$$\mathbf{d} = \sum_{i=1}^N \tilde{h}^i \mathbf{g}^i, \quad (20)$$

180 Therefore, a natural fission-track histogram  $\mathbf{d}$  can be approximated by a weighted sum of interpolated laboratory track length histograms (Fig. 2 and Fig. AB1 in Appendix BA).



185 Figure 2: All randomly oriented tracks start with the length  $L_0$  and then annealed by time and temperature. At present the track length histogram is  $\tilde{h}$ , an idealized histogram without track length broadening effects. The most recent tracks appear in the rightmost column of  $\tilde{h}$ . This histogram is broadened by convolution to mimic the histogram  $d$  resembling a measured histogram. The broadening is caused by **initial length range, biases, and uncertainties**: 1) tracks initially generated with a distribution of lengths, 2) anisotropic annealing, 3) anisotropic etching, and 4) uncertainties of measurement of track lengths. The convolution itself may be regarded as a summation of the broadening of separate columns of  $\tilde{h}$ . Deconvolution removes the broadening of  $d$ .

$g^i$  is a filter transforming the weights  $h^i$  into the natural histogram  $d$ :

$$190 \quad \mathbf{d} = \mathbf{G}\mathbf{h}, \quad (21)$$

or

$$\begin{bmatrix} d^1 \\ d^2 \\ \vdots \\ d^M \end{bmatrix} = \begin{bmatrix} g_1^1 & g_1^2 & \dots & g_1^N \\ g_2^1 & g_2^2 & \dots & g_2^N \\ \vdots & \vdots & \dots & \vdots \\ g_M^1 & g_M^2 & \dots & g_M^N \end{bmatrix} \begin{bmatrix} h^1 \\ h^2 \\ \vdots \\ h^N \end{bmatrix}, \quad (22)$$

Each column of the matrix  $\mathbf{G}$  is a filter with increasing mean track length from column 1 to  $N$ . Solving Eq. (21) for  $\mathbf{h}$  (the model) is named deconvolution. The equation does not take data variance into account. Therefore, a probabilistic inverse method is used (Tarantola, 2005) assuming Gaussian distributions of variance–covariance of data, prior information, and modelization. The solution (the model) is named the posterior  $\tilde{\mathbf{h}}$  (Tarantola, 2005):

$$\tilde{\mathbf{h}} = \mathbf{h}_{prior} + (\mathbf{G}^T \mathbf{C}_D^{-1} \mathbf{G} + \mathbf{C}_H^{-1})^{-1} \mathbf{G}^T \mathbf{C}_D^{-1} (\mathbf{d}_{obs} - \mathbf{G}\mathbf{h}_{prior}). \quad (23)$$

Prior information  $\mathbf{h}_{prior}$  is derived from other independent information or, if not available, simply homogeneous with the elements equal to the mean value of the number of measured tracks.  $\mathbf{C}_D$  is the variance–covariance matrix of the natural observed data  $\mathbf{d}_{obs}$ . The measurements of a given number of track lengths are statistically considered as several possible outcomes of a trial greater than two. The multinomial statistical distribution is therefore used to describe variance–covariance. The diagonal elements of  $\mathbf{C}_D$  are the variances of the observed number of tracks for each length interval.:

$$\mathbf{C}_D(j,j) = DP^j(1-j) \quad \text{for } j = 1 \dots M, \quad (24)$$

where  $P^{ji} = d_{obs}^{ji}/D$  is the probability of the observed data  $d^{ji}$ .  $D$  is the number of measured natural tracks. The off–diagonal elements are the covariances

$$\mathbf{C}_D(l,j) = -DP^l P^j \quad \text{for } l \neq j. \quad (25)$$

Modelization variance caused by the variance of  $\mathbf{G}$ , Eq. (21), is calculated by forward modelling using Eq. (21) and added to  $\mathbf{C}_D$  (Tarantola, 2005). This variance is calculated by random Gaussian realizations of the filters assuming the standard deviations to be  $\sqrt{g^i}$ . The variance–covariance matrix  $\mathbf{C}_H$  for the prior is calculated similarly to  $\mathbf{C}_D$ . When the influence of prior information is unwanted large variance values are given as diagonal elements of the matrix  $\mathbf{C}\mathbf{C}_H$ . The variance–covariance of the posterior is calculated following Tarantola (2005):

$$\tilde{\mathbf{C}}_H = (\mathbf{G}^T \mathbf{C}_D^{-1} \mathbf{G} + \mathbf{C}_H^{-1})^{-1}. \quad (26)$$

An approximation to the observed data  $\mathbf{d}_{obs}$  is calculated forwardly using the posterior:

$$\widetilde{\mathbf{d}}_{obs} = \mathbf{G}\tilde{\mathbf{h}}. \quad (27)$$

The deconvolved histogram  $\tilde{\mathbf{h}}$  is essential for the calculation of track age calculation as discussed below.



#### 4 Equations for the age distribution of corrected tracks

The density  $\sigma^i$  of induced tracks, generated in the time interval  $\Delta t^i$ , intersecting a polished surface plane of the mineral is related to the mean track length (Green et al., 1986). It is here approximated by a logarithmic expression (Appendix CB):

$$\frac{\sigma^i}{\sigma_0^i} = \left[ 1 + \frac{1}{b} \ln \left( \frac{L^i}{L_0} \right) \right], \quad (28)$$

where  $\frac{\sigma^i}{\sigma_0^i}$  is the reduced surface track density,  $\frac{L^i}{L_0}$  is the reduced mean track length, and  $b$  is a calibration constant dependent on the mineral composition. Natural tracks generated in the time interval  $\Delta t^i$  and with a present mean track length  $L^i$  is expected to have the same reduced surface track density as laboratory annealed tracks with the same reduced mean track length. Equation (28) is therefore also valid for the natural tracks. The initial surface track density  $\sigma_0^i$  generated in the time interval  $\Delta t^i$  is expected to be proportional to the initial mean track length and time

$$\sigma_0^i = \frac{1}{2} \xi \lambda_f c L_0 \Delta t^i, \quad (29)$$

where  $\xi$  is a calibration constant. Combining Eq. (28) and Eq. (29) leads to the surface track density assigned to the time interval  $\Delta t^i$ :

$$\sigma^i = \frac{1}{2} \xi \lambda_f c L^i \Delta t^i, \quad (30)$$

where

$$L^i = \left[ 1 + \frac{1}{b} \ln \left( \frac{L^i}{L_0} \right) \right] L_0. \quad (31)$$

The value of  $L^i$ , having the unit of length, is less than the mean track length  $L^i$  and is considered as a correction to the mean track length  $L^i$ . The natural surface track density  $\sigma_s$  is composed of contributions from all the time intervals

$$\sigma_s = \sum_{i=1}^N \sigma^i, \quad (32)$$

Inserting the right side of Eq. (30) instead of  $\sigma^i$  in Eq. (32) leads to

$$\sigma_s = \frac{1}{2} \xi \lambda_f c \sum_{i=1}^N (L^i \Delta t^i). \quad (33)$$

Remembering that  $h^i = \tilde{h}^i$ , Eq.(17), and that the result of the inversion  $\tilde{h}^i$  is an approximation to approximate  $h^i$  we get together with Eq.(14)

$$\sigma_s = \frac{\xi L_0}{2K} \sum_{i=1}^N \left( L^i \sum_{j=1}^M \left( \frac{\tilde{h}^i}{L_j^i} \right) \right). \quad (34)$$

Inserting Eq. (14) for  $\Delta t^i$  into Eq. (30) leads to

$$\sigma^i = \frac{1}{2} \xi \lambda_f c L^i \Delta t^i = \frac{\xi L_0}{2K} L^i \sum_{j=1}^M \left( \frac{\tilde{h}^i}{L_j^i} \right). \quad (35)$$

The ratio between  $\sigma^i$  and  $\sigma_s$  is

$$\sigma^i = \sigma_s \frac{L^i \sum_{j=1}^M \left( \frac{\tilde{h}^i}{L_j^i} \right)}{\sum_{i=1}^N \left( L^i \sum_{j=1}^M \left( \frac{\tilde{h}^i}{L_j^i} \right) \right)}. \quad (36)$$

This equation is used to calculate the surface track density caused by tracks generated in the time interval  $\Delta t^i$  given the surface track density  $\sigma_s$  and the corrected histogram  $\tilde{h}$ . An expression for the time interval  $\Delta t^i$  is obtained combining Eq. (30) and Eq. (36), and isolating the time interval on the left side:

$$\Delta t^i = \frac{2\sigma_s}{\xi\lambda_{fc}} \frac{\sum_{j=1}^M \frac{\tilde{h}_j^i}{L_j^i}}{\sum_{i=1}^N \left( L^i \sum_{j=1}^M \frac{\tilde{h}_j^i}{L_j^i} \right)} \quad (37)$$

The formation time (age) for the oldest corrected track  $t_p$  in each column  $p$  of the histogram  $\tilde{h}$  is the cumulation of the time intervals  $\Delta t^i$  corresponding to the column  $p$  and younger columns.

$$t_p = \sum_{i=p}^N \Delta t^i. \quad (38)$$

That is

$$t_p = \frac{2\sigma_s}{\xi\lambda_{fc}} \frac{\sum_{i=p}^N \sum_{j=1}^M \frac{\tilde{h}_j^i}{L_j^i}}{\sum_{i=1}^N \left( L^i \sum_{j=1}^M \frac{\tilde{h}_j^i}{L_j^i} \right)}. \quad (39)$$

The unit of  $\tilde{h}_j^i$  is number/ $m^3$  but since it appears both in the nominator and denominator  $\tilde{h}_j^i$  can as well be considered dimensionless. Therefore, the volume need not be measured. The decreasing uranium concentration through time is considered by introducing the logarithm in Eq. (39).

$$t_p = \frac{1}{\lambda_D} \ln \left( 1 + \frac{2\sigma_s\lambda_D}{\xi\lambda_{fc}} \frac{\sum_{i=p}^N \sum_{j=1}^M \frac{\tilde{h}_j^i}{L_j^i}}{\sum_{i=1}^N \left( L^i \sum_{j=1}^M \frac{\tilde{h}_j^i}{L_j^i} \right)} \right), \quad (40)$$

where  $\lambda_D$  is the total decay constant. The corresponding surface track density is

$$\sigma_p = \sum_{i=p}^N \sigma^i, \quad (41)$$

and using Eq. (36)

$$\sigma_p = \sigma_s \frac{\sum_{i=p}^N L^i \sum_{j=1}^M \frac{\tilde{h}_j^i}{L_j^i}}{\sum_{i=1}^N \left( L^i \sum_{j=1}^M \frac{\tilde{h}_j^i}{L_j^i} \right)}. \quad (42)$$

Equation (39) and Eq. (42) are valid for tracks selected within a given angle from the horizontal. Equations for the case when tracks are selected following the requirement that both ends are in focus at the same time are given in Appendix DC.

Inversion following Eq. (23) applies both for data measured in the old-fashioned way where track angle to the c-axis is not measured as well as for new measurements which include the angle, Appendix EB.

### 5.3 Variance of ages

The oldest age  $t_p$  of corrected tracks in column  $p$  given by Eq. (39) and repeated here:

$$t_p = \frac{2\sigma_s}{\xi\lambda_f c} \frac{\sum_{i=p}^N \sum_{j=1}^M \left(\frac{A_j^i}{L_j^i}\right)}{\sum_{i=1}^N \left(L^i \sum_{j=1}^M \left(\frac{A_j^i}{L_j^i}\right)\right)} \quad (43)$$

and approximately

$$t_p \approx \frac{2\sigma_s}{\xi\lambda_f c} \frac{\sum_{i=p}^N \left(\frac{A_i^i}{L_i^i}\right)}{\sum_{i=1}^N \left(L^i \frac{A_i^i}{L_i^i}\right)} \quad (44)$$

The variance of  $t_p$  is derived by the linear approximation

$$t_p(\mathbf{x}) \approx t_p(\mathbf{x}_0) + \mathbf{J} \cdot \Delta \mathbf{x}, \quad (45)$$

where  $\mathbf{x}_0$  is the vector with the elements  $\sigma_s, \xi, \lambda_f, c, \sum_{i=p}^N \left(\frac{A_i^i}{L_i^i}\right), \sum_{i=1}^N \left(L^i \frac{A_i^i}{L_i^i}\right)$ .  $\mathbf{J}$  is the Jacobian calculated numerically, and  $\Delta \mathbf{x} = \mathbf{x} - \mathbf{x}_0$ .

The variance-covariance matrix of  $t_p$  is then

$$\mathbf{C}_t = \mathbf{J} \mathbf{C}_x \mathbf{J}^T \quad (46)$$

where  $\mathbf{C}_x$  is the variance-covariance matrix of  $\mathbf{x}$ . The variances of the oldest ages of the corrected tracks are the diagonal elements of  $\mathbf{C}_t$ .

through the variance of the three parts  $f_x, f_y,$  and  $f_z$  of the equation:

$$f_x = \frac{2\sigma_s}{\xi\lambda_f c}, \quad (45)$$

$$f_y(p) = \sum_{i=p}^N \left(\frac{A_i^i}{L_i^i}\right), \quad (46)$$

$$f_z = \sum_{i=1}^N \left(L^i \frac{A_i^i}{L_i^i}\right). \quad (47)$$

The age of the oldest track in column  $p$  is then

$$t_p \approx f_x \frac{f_y(p)}{f_z}. \quad (48)$$

The variance of each part is calculated using standard textbook statistics. The variance of  $f_x$  is

$$\text{Var}(f_x) = \left(\frac{\partial f_x}{\partial \sigma_s}\right)^2 \cdot \text{Var}(\sigma_s) + \left(\frac{\partial f_x}{\partial \xi}\right)^2 \cdot \text{Var}(\xi) + \left(\frac{\partial f_x}{\partial \lambda_f}\right)^2 \cdot \text{Var}(\lambda_f) + \left(\frac{\partial f_x}{\partial c}\right)^2 \cdot \text{Var}(c) \quad (49)$$

The second part  $f_y$  is a cumulation of correlated histogram columns  $\frac{A_i^i}{L_i^i}$ . The variance of  $f_y$  therefore includes the covariance:

$$\text{Var}(f_y(p)) = \sum_{i=p}^N \text{Var}\left(\frac{A_i^i}{L_i^i}\right) + 2 \sum_{\substack{i < j \\ i, j \in M}} \text{Cov}\left(\frac{A_i^i}{L_i^i}, \frac{A_j^j}{L_j^j}\right) \quad (50)$$

$$Var(f_z(p)) = \sum_{i=p}^N \frac{1}{L_i^2} Var(A^i) + 2 \sum_{p \leq i < j \leq N} \frac{1}{L_i L_j} Cov(A^i, A^j) \quad (51)$$

The variance of  $f_z$  is

$$Var(f_z) = \sum_{i=1}^N Var(L_i \frac{h^i}{L_i}) = \sum_{i=1}^N L_i^2 Var\left(\frac{h^i}{L_i}\right) + \left(\frac{h^i}{L_i}\right)^2 Var(L_i) \quad (52)$$

where

$$Var(L_i) = (L_0 \ln\left(\frac{L_i}{L_0}\right))^2 \frac{1}{b^2} Var(b). \quad (53)$$

The equation for the age, Eq. (48) repeated, is written in terms of the three parts

$$t_p = f_z \frac{f_z(p)}{f_p}. \quad (54)$$

The variance of  $t_p$  is then

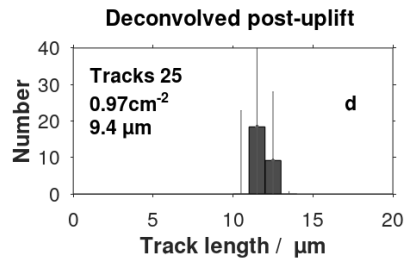
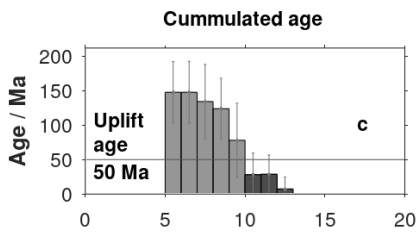
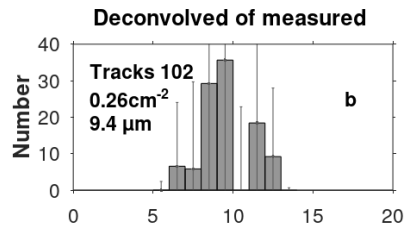
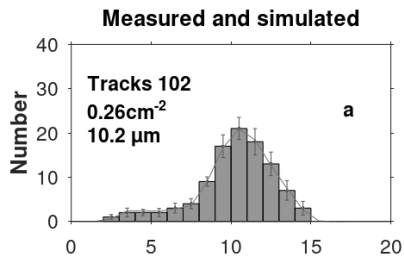
$$Var(t_p) = \left(\frac{f_z(p)}{f_p}\right)^2 Var(f_z) + \left(\frac{f_z}{f_p}\right)^2 Var(f_z(p)) + \left(\frac{f_z(p)}{f_p}\right)^2 Var(f_z). \quad (55)$$

## 6 Testing the deconvolution method

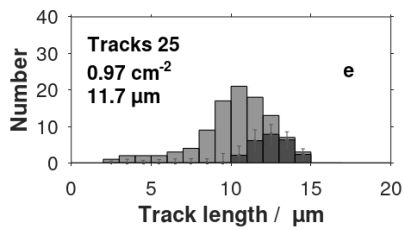
Deconvolution is a mathematical tool capable of reducing noise and correct for biases in time series such as seismic signals.

We, therefore, expect that deconvolution can reduce the length spread of confined horizontal fission tracks. This is shown in the following example. Assume that a sample starts generating tracks at a temperature of 63 °C, 150 Ma back in time. At 50 Ma it is suddenly uplifted to a temperature of 20 °C until the present. The corresponding track length histogram is calculated forwardly resulting in the histogram seen in Fig. 3a. The track length annealing model by Stephenson et al. (2006) is used. This synthetic histogram is like a measured histogram. The two temperature plateaus experienced by the sample is expected to result in a bimodal track length histogram. However, the spread of tracks blurs this impression. After deconvolution of the synthetic histogram the bimodality is revealed, Fig. 3b. The deconvolution succeeds because the filters used (Appendix B) are not completely covering each other. Each column of the deconvolved histogram (Fig. 3b) is converted to the time it takes to generate the tracks belonging to them, Eq. (37). The age histogram in Fig. 3c is obtained by summing up the time intervals from the most recent to the oldest. Imagine that the time of the uplift at 50 Ma is known from other sources. The expected post-uplift tracks of the deconvolved histogram are those with ages below the 50 Ma line, coloured dark gray in Fig. 3c. Convolution of the post-uplift deconvolved histogram (Fig. 3d) show the post-uplift tracks of the synthetic histogram, Fig. 3e. Convolution is the opposite of deconvolution having the effect of broadening track length histograms.

Commented [PK11]: Old version.



**Measured, Convolved of deconvolved post-uplift**



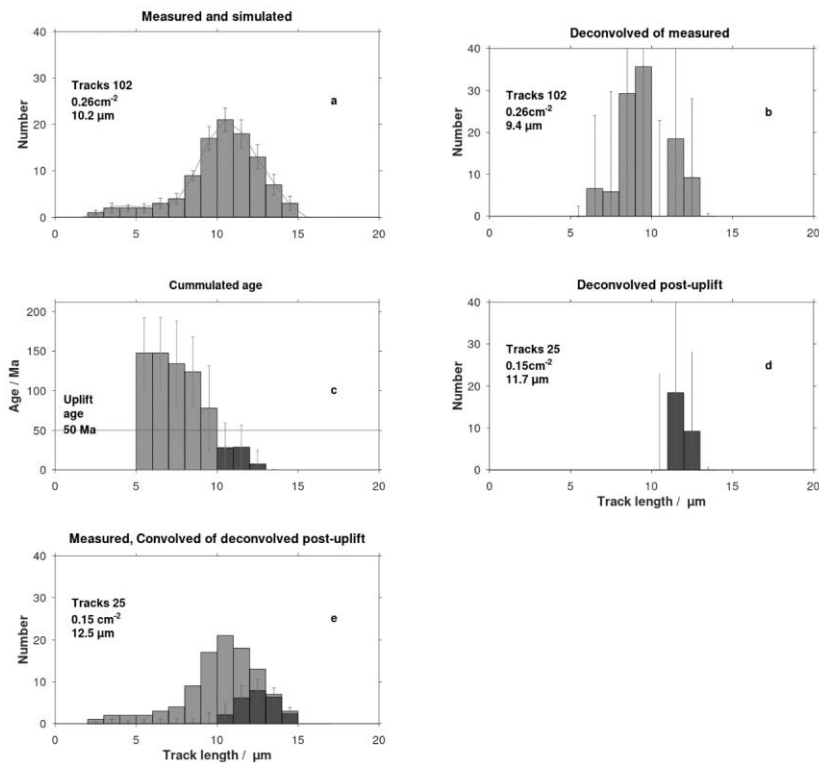


Figure 3: (a) is the forward simulated track length histogram like a measured histogram; (b) The deconvolved histogram of the measured histogram; (c) The cumulated age histogram. The dark gray columns identifies the post-depositional tracks; (d) The post-uplift columns of the deconvolved histogram; (e) Convolution (spreading out) of the deconvolved post-uplift histogram, is like the post-uplift part (coloured dark gray) of a measured track length histogram.

#### 74 Inherited tracks

The deconvolution technique can be used to extract the post-depositional part of track length histograms with inherited tracks. This is illustrated in Fig. 43 by a simplified idealized (no broadening) model for track annealing and observation. Grains

from two source areas are considered. There are more tracks in the post-depositional columns of Grain 2 than in Grain 1 because it is assumed that the uranium content of Grain 2 is twice that of Grain 1. The two post-depositional columns of Grain 1 and 2 represent the same two time intervals. For both Grain 1 and 2, there is one column where pre- and post-depositional tracks are mixed. This column and the pre-depositional columns of both grain types do not necessarily represent the same time intervals because their different thermal histories create individual track length distributions (histograms). The pre-depositional tracks of Grain 1 compared with those of Grain 2 have experienced different thermal histories and therefore different degree of annealing. Post-depositional tracks are ordered with decreasing length as a function of time in contrast to the pre-depositional tracks which may be disordered. Fig. 34C sums Grain 1 and 2 histograms. It is observed that the post-depositional time intervals for the bulk histogram are identical to those for the two separate grain types. The age equation, Equation (40), is valid for post-depositional corrected tracks but not for mixed or pre-depositional -tracks.

335

340

345

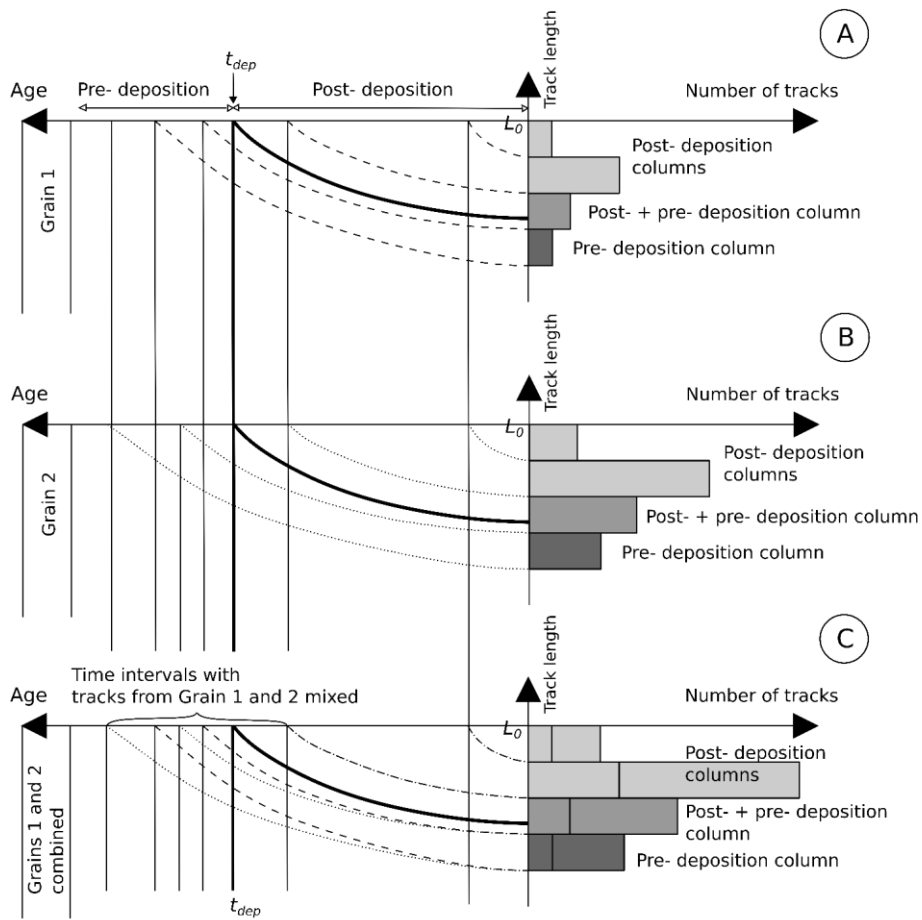




Figure 34: Sketch for the accumulation of **simplified** tracks in histogram columns. All tracks start with the length  $L_0$ . Some tracks are generated before deposition and some after. The actual track lengths are reduced as a function of time; (A) Grain 1; (B) Grain 2 which has experienced a different pre-depositional thermal history; (C) Histogram for the bulk of Grain 1 and 2.

The post-depositional part of the deconvolved histogram  $\tilde{h}$  are the columns having track ages  $t_p$  less than the deposition age  $t_{dep}$ :

$$t_p \leq t_{dep}, \quad (56)$$

where  $p$  is the column number. Together with Eq. (40), we obtain

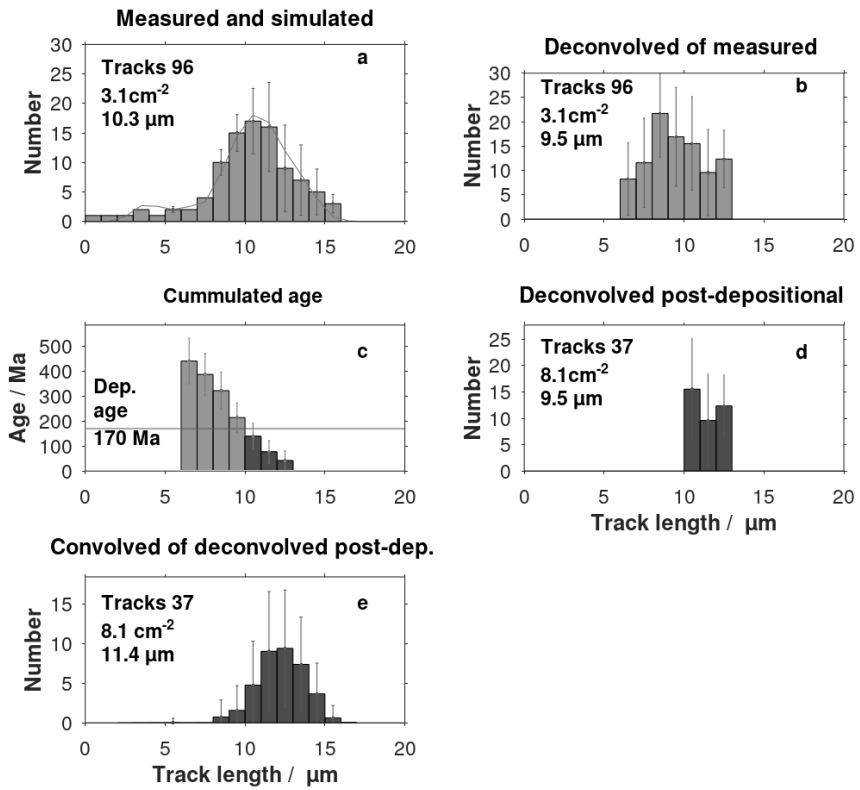
$$\frac{1}{\lambda_D} \ln \left( 1 + \frac{2\sigma_s \lambda_D}{\xi \lambda_{fc}} \frac{\sum_{i=p}^N \sum_{j=1}^M \left( \frac{\hat{h}_j^i}{L_j^i} \right)}{\sum_{i=1}^N \left( L^i \sum_{j=1}^M \left( \frac{\hat{h}_j^i}{L_j^i} \right) \right)} \right) \leq t_{dep}. \quad (57)$$

The values of  $p$  satisfying the inequality identifies the post-sedimentary columns. The smallest number of  $p$  identifies the oldest post-sedimentary track. This number is used to calculate the surface track density  $\rho_{post}$  linked to the post-depositional histogram by Eq. (42):

$$\sigma_{post} = \sigma_s \frac{\sum_{i=p_{post}}^N L^i \sum_{j=1}^M \left( \frac{\hat{h}_j^i}{L_j^i} \right)}{\sum_{i=1}^N \left( L^i \sum_{j=1}^M \left( \frac{\hat{h}_j^i}{L_j^i} \right) \right)}. \quad (58)$$

Summations are performed for all columns representing the post-sedimentary history. Together with the surface track density  $\sigma_{post}$  the post-depositional histogram may be used to calculate the post-depositional thermal history applying the backward modeling procedure described by Jensen et al. (1992). Alternatively, the post-depositional de-convolved histogram can be convolved by forward calculation by Eq. (27) and used by random or guided-random search algorithms (Lutz and Omar, 1991; Willett, 1997; Ketcham, 2005; Gallagher, 1995; 2012).

Identification of post-sedimentary fission-tracks is exemplified by applying apatites from the sample GGU103113 (Jameson Land, East Greenland). The Middle Jurassic sandstone sample (170 Ma) has the apparent fission-track age 245 Ma (Hansen et al., 2001). The measured and the deconvolved track length distributions are shown in Fig. 45a and 45b.



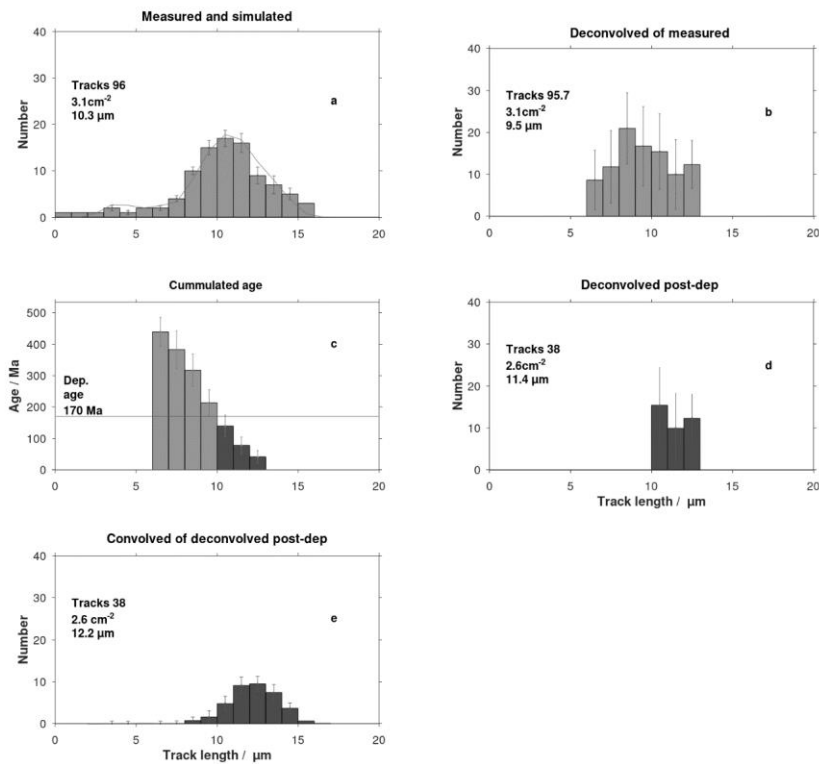


Figure 45: Extraction of the post-sedimentary part of a track length histogram from Jameson Land, East Greenland (Hansen, 1996). The unit of surface track density is  $\text{cm}^{-2}$ . (a) Measured and simulated (thin line) fission-track length histogram; (b) The histogram after deconvolution using the filters shown in Appendix BA; (c) Ages of corrected tracks are calculated by Eq. (40) using the deconvolved histogram. The columns (dark grey) with ages of corrected tracks ages less than the deposition age (170 Ma) are identified; (d) The post-sedimentary histogram is extracted from the deconvolved histogram based on the identified post-depositional columns. This histogram is the basis for direct calculation of the temperature history (Jensen et al., 1992); (e) The convolved post-sedimentary histogram, resembling a measured histogram, can be used by Monte Carlo type simulation models (Ketcham, 2005; Gallagher, 1995).

The parameter  $\xi$  in the age equation, Eq. (40) is adjusted to 0.752 (with  $b = 0.784$ ) to obtain simulated apparent age equal to the apparent age reported by Hansen et al. (2001). The apparent age is calculated using a track length distribution of an unannealed track length distribution in Eq. (40). The post-depositional columns are identified as being the rightmost columns

with accumulated ages of corrected tracks less than the deposition age, Fig. 45c and Fig. 45d. The deconvolved histogram Fig. 45d can be used to calculate the post-sedimentary thermal history. The histogram in Fig. 45e is the convolution of the histogram in Fig. 45d.

## 385 **85 Discussion**

The equations for accumulated fission-tracks derived here are based on the practice of selecting horizontal tracks for length measurements. We follow the recommendation by Ketcham (2019) who selects all tracks within  $\pm 10^\circ$  from the horizontal. Alternatively, Gleadow et al. (1986b) and Galbraith (2005) select tracks observed in reflected light being within  $\pm 10^\circ$  from the horizontal and with both ends in focus in transmitted light. Fewer long tracks ( $> 8.5 \mu\text{m}$ ) are then selected relatively to shorter tracks (Appendix DC). An alternative set of equations are given in Appendix DC for this situation.

Standard deviations of the ages are calculated based on the variance of input data, prior model, and modelization. The calculated deviations are high but they agree with deviations of histograms reported in an interlaboratory comparison (Ketcham et al., 2009). It is required that the laboratory annealed tracks are measured in the same way as the natural tracks. E.g., in the Jameson Land example, the recommendations by Gleadow et al., (1986b) and Gleadow et al., (2019) are used in both cases.

The inversion procedure by Tarantola (2005) requires a prior model being independent of data. As the default, a prior model histogram with an equal number of tracks in the columns is chosen. In some cases, negative track length histogram columns appear as a result of inversion because due to unrealistic data. An improved prior model based on other information is then necessary. The problem can be managed by smoothing of input data and/or of covariance matrices.

When track angles to the c-axis is available it is common practice to calculate the histogram of the c-axis projected tracks. However, detailed information on track density is lost along the accumulation along the projection path. Instead, one can use 3D-track length histograms as described in Appendix ED. 3D-histograms do not involve projections and therefore retain both length and angle information. The inversion procedure presented here is valid for both 2D- and 3D-histograms (Appendix ED).

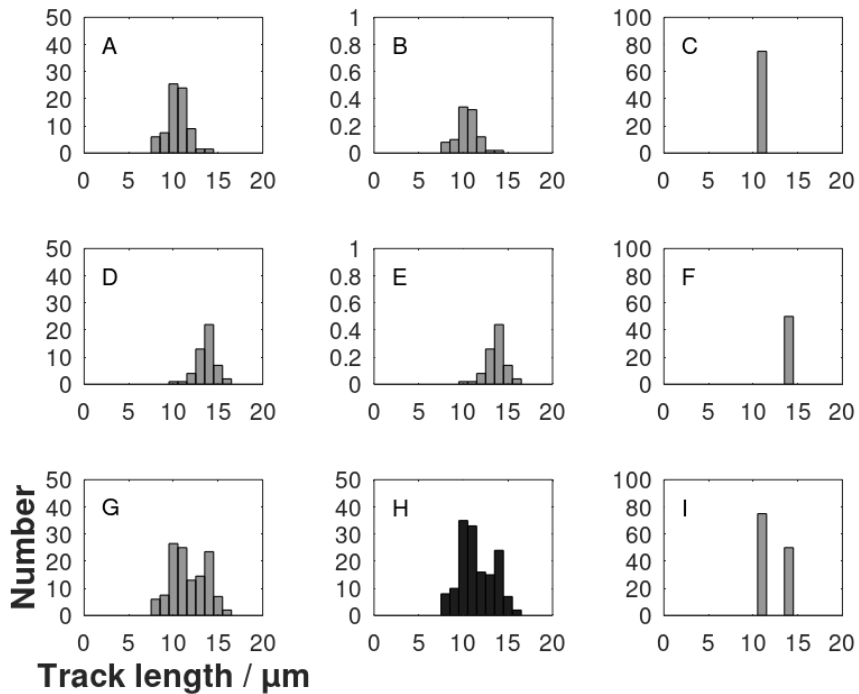
## 96 Conclusions

As an example, the deconvolution method presented here is used to identify the post-depositional part of a track length histogram from Jameson Land, Greenland. A new procedure for deriving ages of corrected fission-tracks ages as a function of track length is suggested. The natural fission-track length histogram is considered as linearly composed of histograms of induced tracks partially annealed in the laboratory. Inversion is performed by a probabilistic inverse theory. The resulting ages

of corrected tracks ages are given as centers of posterior with variance. The equations are valid for old-type measurements where the track angle to the c-axis is not measured as well as for recent data including measurements of the angle to the c-axis. Data with both track lengths and angles are organized in 3D-histograms presented as images. Two types of track length measurements are discussed. If tracks with both ends in focus are selected there is a tendency to off-select longer tracks. If all tracks within a given angle are selected this bias disappears. The equations presented here are prepared for both cases. The calculation of the ages of corrected tracks ages does not require the calculation of the sample thermal history. Instead, they are the basis for temperature history calculation. ~~As an example, the deconvolution method presented here is used to identify the post-depositional part of a track length histogram from Jameson Land, Greenland.~~

#### Appendix A

After the formation of the unetched randomly oriented tracks, the spreading of lengths increases during the process of annealing leading to a considerable mixing of lengths of the observed track length histogram. There is not a unique relationship between time and the length of individual tracks. However, the relationship is not completely blurred. There is a tendency that old tracks appear in the short track length part of the histogram and young tracks in the opposite part. To some extent, deconvolution can reduce the spread. Deconvolution is used extensively in seismic processing to improve the signal-to-noise ratio and remove biases. This requires the character of the noise to be known. The "noise" in connection with fission tracks is the spread observed in laboratory annealing experiments. This is used to reduce the spread of the observed track length histograms. That is, the observed histogram can be deblurred by deconvolution. A simplified demonstration of deconvolution of a bimodal track length histogram is shown in Fig. A1. The present paper applies a more advanced least squares deconvolution technique.



435 **Figure A1:** Illustration of deconvolution of a track length histogram. The dark gray histogram H is the observed histogram. The histogram I is an initial guess of a deconvolved histogram with 80 and 50 tracks in each column. The histograms F and C are the two columns of histogram H separated. The histograms B and E are normalizations of histograms observed after track annealing in the laboratory. They are named filters. Histogram A is histogram B multiplied by the number of tracks in histogram C. Histogram D is histogram E multiplied by the number of tracks in histogram F. Histogram G is histogram A plus histogram D. Histogram G is then the result of convolution of histogram I with the filters B and E. The synthetic histogram G is compared with the observed histogram H however, the left part is dissimilar. Therefore, the suggested deconvolved histogram I is not successful.

445 A successful deconvolution is shown in Fig. A2. The spread of tracks in the bimodal histogram H is assembled in two columns corresponding to two thermal time periods. Note that two time periods can be separated despite the track length overlap of the histograms A and D. The deconvolved track length histogram I is arranged according to time. Each column can be converted to an equivalent time interval. The age of the oldest track of each deconvolved histogram is calculated by adding its time interval and younger time intervals. In this process there has been no use of a track annealing model.

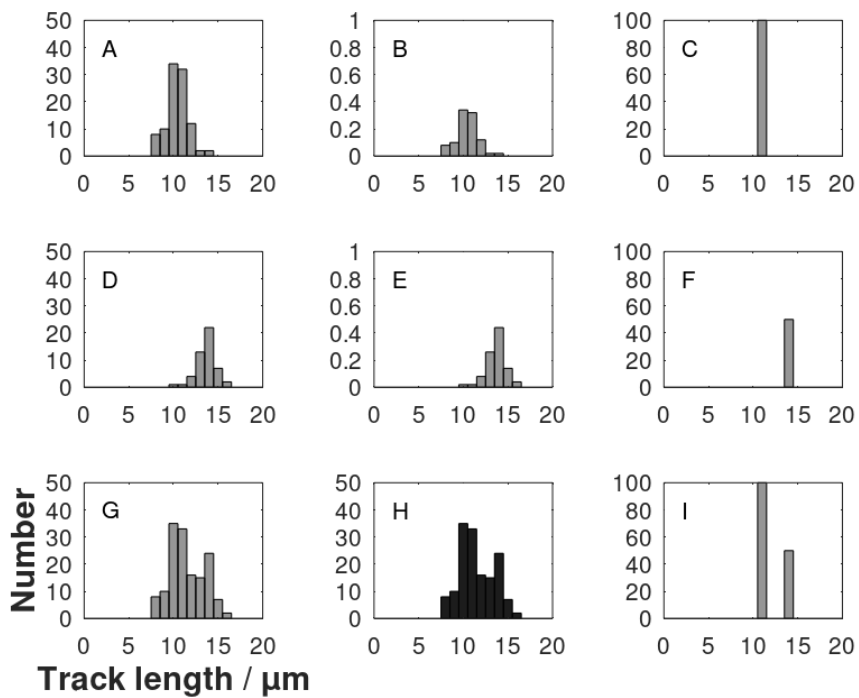
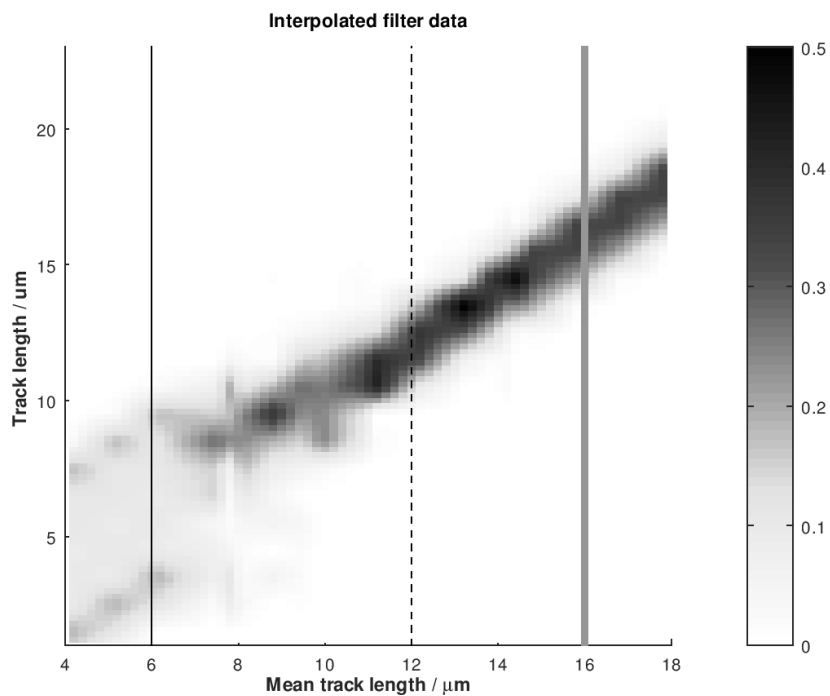


Figure A2: The final step of the deconvolution procedure showing the successful deconvolution of histogram H. Histogram I is the deconvolved histogram. The degree of success is measured by comparing the convolved histograms G and histogram H.

#### Appendix BA

The filters used for deconvolution are the columns of matrix **G**, Eq. (22). They are based on measurements of track lengths after annealing in the laboratory (Gleadow et al., 1986a; Green et al., 1986; Barbarand et al., 2003). The histograms of these track lengths are normalized by division with the number of tracks of each histogram. They represent the probability of an

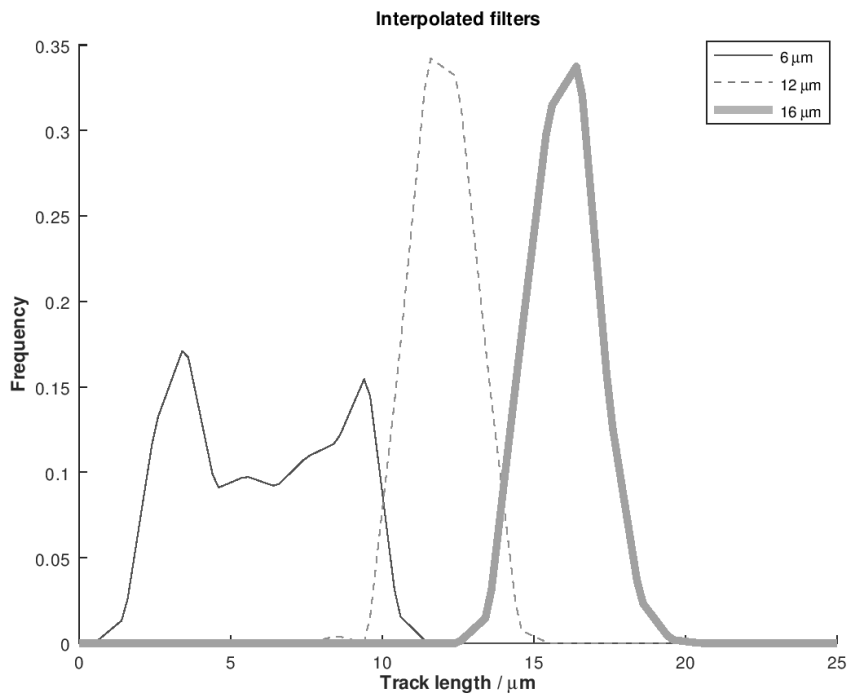
induced track ~~to~~-appearing in a certain length interval. Interpolated filters are obtained using a mesh of  $0.2 \mu\text{m}$  in both directions (bins and mean track lengths), Fig. AB1.



460 Figure AB1-; Interpolation of the filters used for deconvolution. It is based on track annealing in the laboratory (Gleadow et al., 1986a; Green et al., 1986; Barbarand et al., 2003). Three linear intersections are shown in Fig. AB2. Grayscale is frequency.

The filters broaden with decreasing mean track length. The columns of the modelization matrix  $G$  are picked from the interpolation. The number of columns is related to the resolution. Fig. AB2 shows three filters extracted from Fig. AB1.





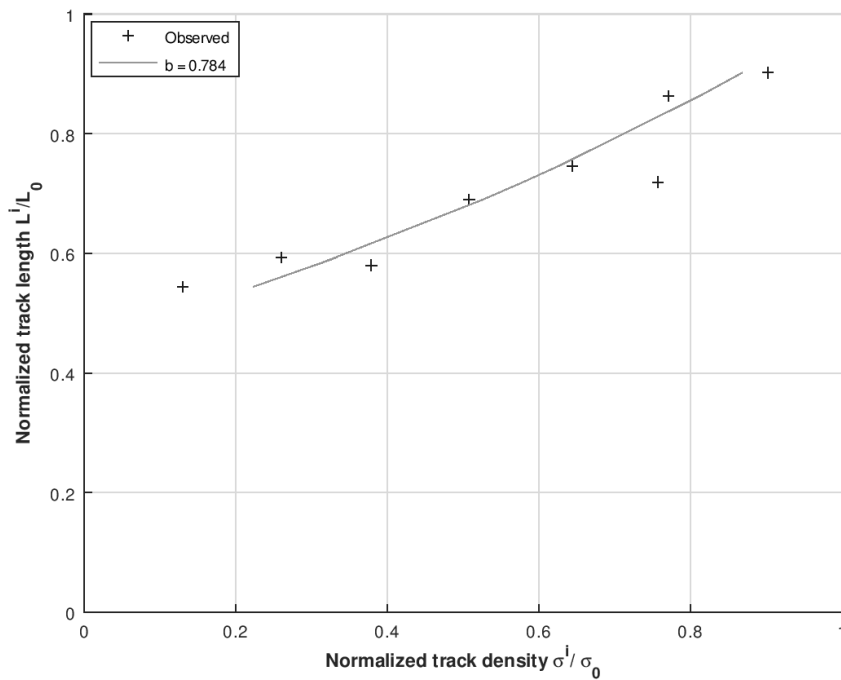
465 **Figure AB2:** Three interpolated filters with mean track lengths 6, 12, and 15 μm extracted from Fig. AB1.

### Appendix BC

Plots of mean track length versus surface track density for tracks generated by neutron radiation and annealed in the laboratory are given by Green et al. (1986). A logarithmic expression approximates data, Fig. BC1:

$$\frac{\sigma^i}{\sigma_0^i} = \left[ 1 + \frac{1}{b} \ln \left( \frac{L^i}{L_0} \right) \right], \quad (\text{AC1})$$

470 where  $\sigma^i / \sigma_0^i$  is the surface track density of partially annealed tracks relative to that of unannealed tracks.  $L^i / L_0$  is the mean track length of partially annealed tracks relative to the unannealed mean track length. Equation (AC1) is used to parameterize the measured data leading to  $b = 0.748 \pm 0.048$  for multi-compositional apatite and  $b = 0.963$  for mono-compositional apatite.  $b$  determines the curvature of the approximating line in Fig. BC1.



475 **Figure BC1:** Parameter  $b$  characterizes the relation between normalized track length  $L^i/L_0$  and normalized density  $\sigma^i/\sigma_0$  for multi-compositional apatite. Data from Green et al. (1988).

#### Appendix ED

Ketcham (2019) recommends the selection of all etched tracks being within  $\pm 10^\circ$  from the horizontal. It is expected that the likelihood of tracks being etched is proportional to their length. This view has been adopted in the main text of this paper.

480 Alternatively to the selection criteria by Ketcham (2019), Gleadow et al (2019) select etched tracks that are within  $10^\circ$ – $15^\circ$  from the horizontal and with both ends in focus at the same time. The two criteria are examined in this appendix.

The axial (vertical) resolution of a light microscope is

$$r_{axial} = 1.4\lambda\eta/NA^2. \quad (\text{ED1})$$

485 With typical values for wavelength of  $\lambda = 550$  nm (green light), refraction index of oil  $\eta = 1.51$ , and numerical aperture  $NA =$   
 1.25, the axial resolution  $r_{axial} = 0.74$   $\mu\text{m}$ . The numerical aperture is a measure of the maximum angle for which the  
 microscope receives light. The criteria by Gleadow et al (2019) imply that a short track, 6  $\mu\text{m}$  long, is accepted for counting if  
 the angle to the horizontal is less than  $10^\circ$ . A long track, 18  $\mu\text{m}$ , has to be within  $2.5^\circ$  to the horizontal to be accepted. The  
 tendency is therefore that long tracks are off-selected from counting. The likelihood of selection is then inverse proportional  
 490 to the track length for tracks longer than 6  $\mu\text{m}$ . At the same time, the likelihood of a horizontal track being etched is expected  
 to be proportional to its length. These two biases essentially cancel each other (Jensen et al., 1992). With the focus window  
 selection criteria (Gleadow et al., 2019) the set of age equations is then:

$$t_p = \frac{1}{\lambda_D} \ln \left( 1 + \frac{2\sigma_s \lambda_D}{\xi \lambda_f c} \frac{\sum_{i=p}^N \tilde{h}^i}{\sum_{i=1}^N (\mathcal{L}^i \tilde{h}^i)} \right) \quad (\text{E}2)$$

The age of the oldest track is obtained summing all the time intervals:

$$t_{max} \sim \frac{2\sigma_s}{\xi \lambda_f c} \frac{\sum_{i=1}^N \tilde{h}^i}{\sum_{i=1}^N (\mathcal{L}^i \tilde{h}^i)}. \quad (\text{E}3)$$

Introducing the mean track length of the inverted histogram  $\tilde{\mathcal{L}}$ :

$$\mathcal{L}_{mean} = \frac{\sum_{i=1}^N (\mathcal{L}^i \tilde{h}^i)}{\sum_{i=1}^N \tilde{h}^i}. \quad (\text{E}4)$$

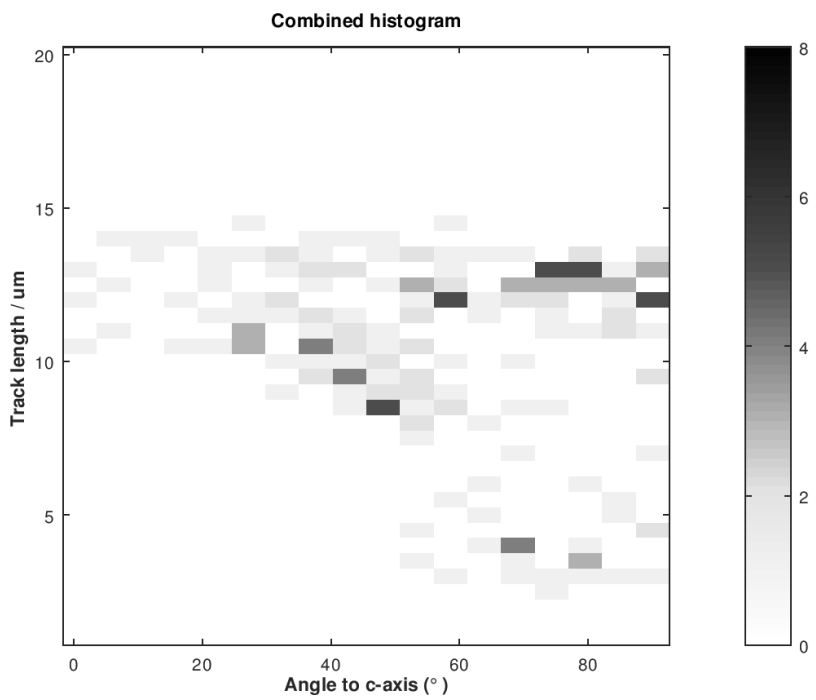
The age of the oldest observable track is

$$t_{max} = \frac{2\sigma_s}{\xi \lambda_f c \mathcal{L}_{mean}}, \quad (\text{E}5)$$

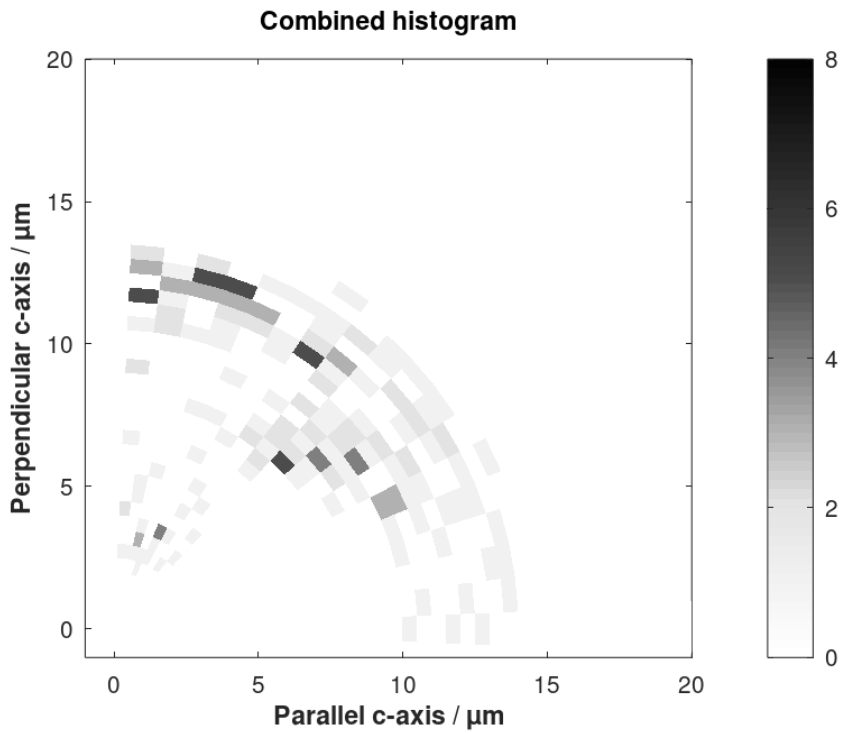
500 equivalent to the derivation by Jensen et al. (1992) when  $\mathcal{L}_{mean}$  is replaced by the mean track length.

## Appendix DE

The inversion principle presented in the main text is for 2D-track length histograms ignoring track angles to the c-axis.  
 However, the inversion principle is also applicable to data that includes the angles. The measured data vector  $\mathbf{d}_{obs}$  in Eq.  
 (2322) is then derived from a 3D-histogram (length, angle, and number). The elements of the vector  $\mathbf{d}_{obs}$  is obtained by  
 505 sequentially numbering each bin (Tarantola, 2005). An example is shown in Fig. DE1 with a synthetic 3D-histogram as data  
 obtained from two annealing experiments.



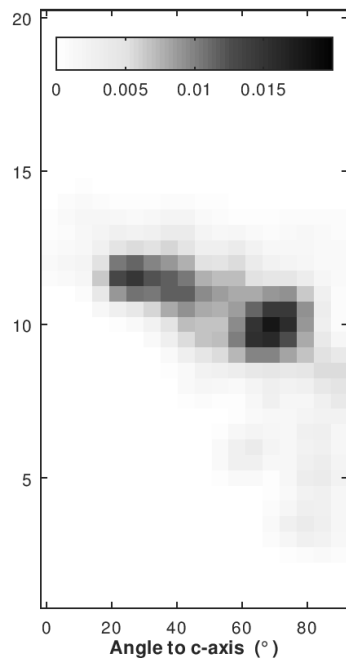
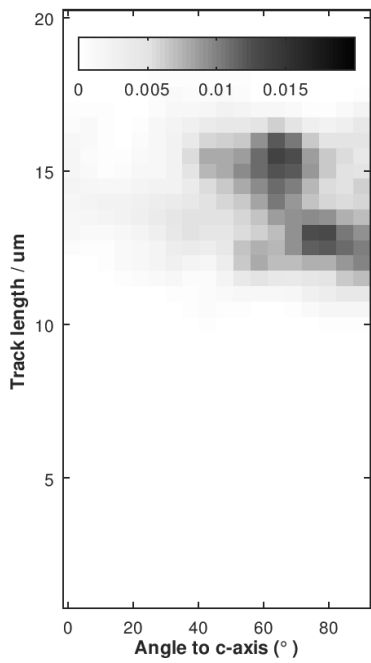
Commented [PKJ3]: Old version



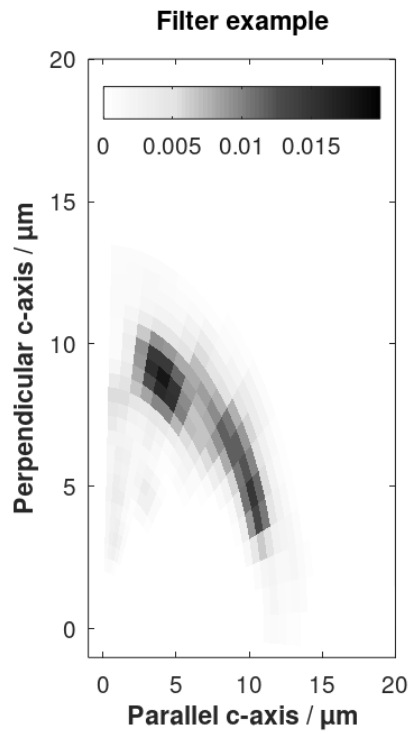
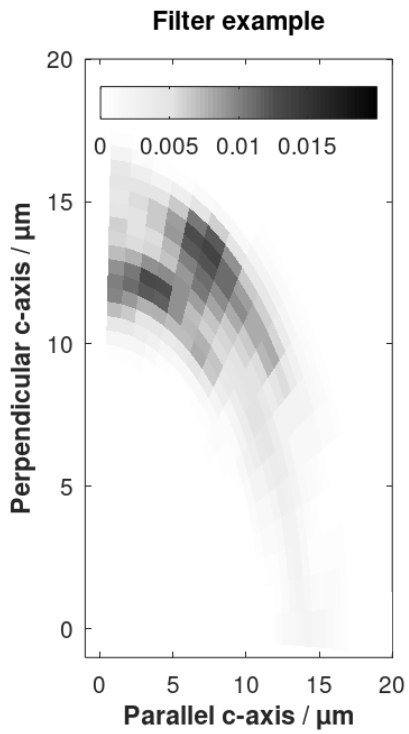
510 Figure DE1: 3D-histogram of track lengths versus angles derived by combining two annealing experiments (Barbarand et al., 2003). Grayscale is the number of tracks in each bin.

They are the result of heating to 275°C and 320°C respectively (Barbarand et al., 2003). Each bin of the 3D-histogram is 5° times 0.5 μm. The matrix  $\mathbf{G}$ , Eq. (22) consists of twenty 3D-filters interpolated between the six annealing experiments by

515 Barbarand et al. (2003). Each column of  $\mathbf{G}$  is a filter. Two of them are shown in Fig. DE2.



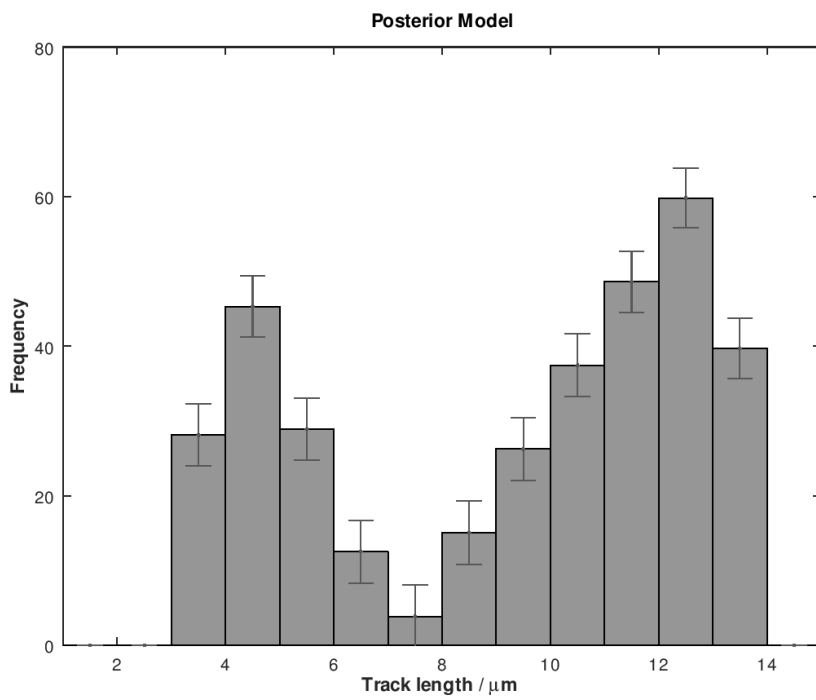
Commented [PK14]: Old version



520

Figure DE2: Examples of 3D-filters used for deconvolution. They are based on heating to 275°C and 320°C respectively, Barbarand et al. (2003). Greyscale is frequency.

The corrected histogram as a result of the inversion using Eq. (2322) is shown in Fig. DE3.



Commented [PKJ5]: Old version



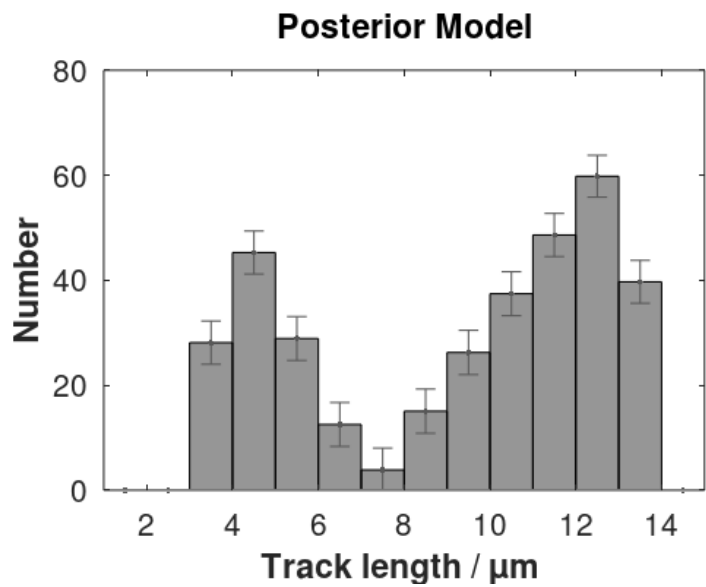
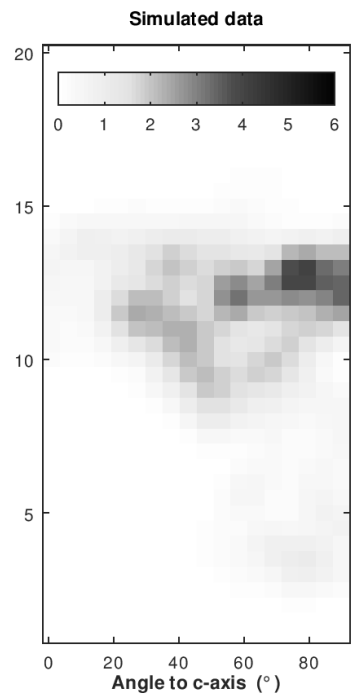
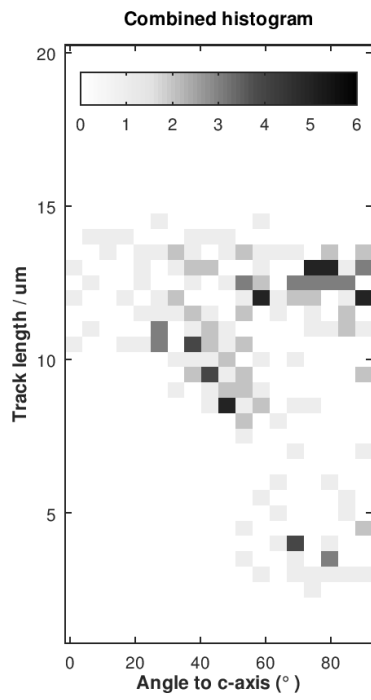
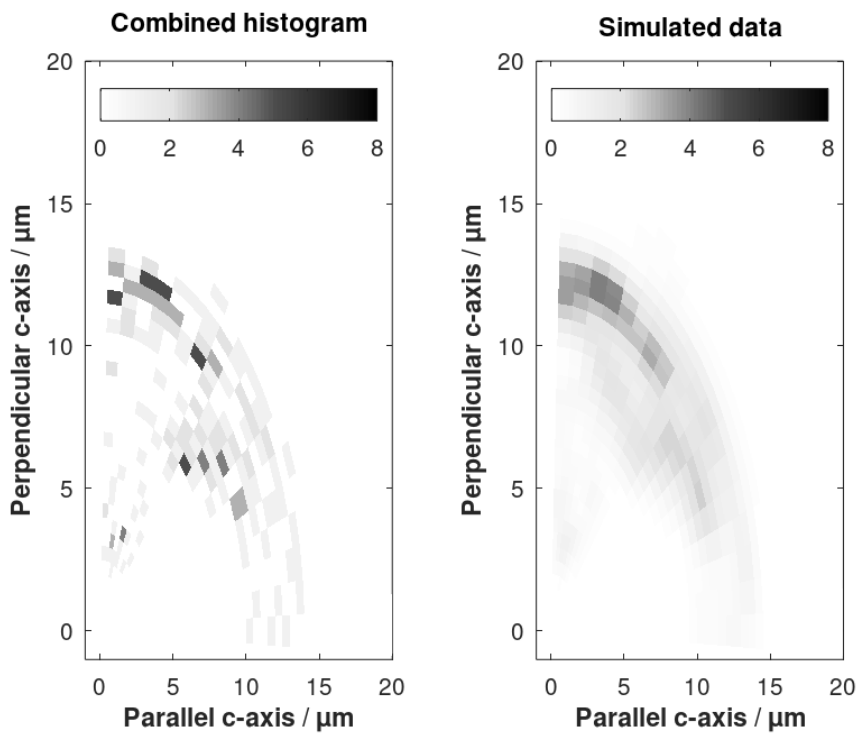


Figure DE3: The corrected histogram as a result of the inversion of the 3D-histogram shown in Fig. DE1.

530 The standard deviations are the diagonal values of the posterior covariance matrix. The result of the inversion is evaluated by comparing forward modeling using Eq. (21) with the inverted histogram as input data (Fig. DE34). Compliance is good.



Commented [PKJ6]: Old version



535

Figure DE4: The combined 3D-histogram considered as synthetic data (Fig. DE1) and the forwardly simulated approximation using the posterior model in Eq. (2324). Grayscale is the number of tracks.

#### Code availability

Octave codes for reproducing the results shown in Fig. AB1, B2, and D1–D4 are available online on Zenodo

540

(<http://doi.org/10.5281/zenodo.5137192> (<https://doi.org/10.5281/zenodo.4553144>; Jensen, 2021a) and (<https://doi.org/10.5281/zenodo.5137293>; Jensen, 2021b) for 2D- and 3D-histograms respectively.

#### **Authors/Author's contribution**

PJ developed the theory. During this process discussion with KH were important. PKJ wrote the equations, and the computer programmes. He also wrote the paper in tight dialog with KH. KH measured track lengths and surface track density used in the example shown in Fig. 45.

#### **Competing interests**

The authors declare that they have no conflict of interest.

#### **References**

Afra, B., Lang, M., Rodriguez, M. D., Zhang, J., Giulian, R., Kirby, N., Ewing, R. C., Trautmann, C., Toulemonde, M., and Kluth, P.: Annealing kinetics of latent particle tracks in Durango apatite, Phys. Rev. B, 83, 6, 064116, <https://doi.org/10.1103/PhysRevB.83.064116>, 2011.

Barbarand, J., Hurford, T., and Carter, A.: Variation in apatite fission-track length measurement: implications for thermal history modelling, Chem. Geol., 198, 1-2, 77-10, doi:10.1016/S0009-2541(02)00423-0, 2003.

~~Belton, D. X., and Raab, M. J.: Cretaceous reactivation and intensified erosion in the Archean-Proterozoic Limpopo Belt: demonstrated by apatite fission-track thermochronology, Tectonophysics, 480, 1-4, 99-108, doi:10.1016/j.tecto.2009.09.018, 2010.~~

Bertagnolli, E., Keil, R., and Pahl, M.: Thermal history and length distribution of fission tracks in apatite, Part I., Nucl. Tracks Radiat. Meas. (1982), 7, 4, 163-177, doi:10.1016/0735-245X(83)90026-1, 1983.

~~Donelick, R. A. Etchable fission track length distribution in apatite: experimental observations, theory and geological applications. Ph.D. dissertation, Rensselaer Polytechnic Institute, Troy, New York, 414 p., 1988.~~

Donelick, R. A., Ketcham, R. A., and Carlson, W. D.: Variability of apatite fission-track annealing kinetics: II. Crystallographic orientation effects, Am Min, 84, 9, 1224-1234, doi:10.2138/am-1999-0902, 1999.

Fleisher, R. L., Price, P. B., and Walker, R. M.: Nuclear Tracks in Solids: Principles and Applications, University of California Press, Berkeley, CA., 1975.

Galbraith, R. F.: Statistics for fission track analysis, Chapman and Hall/CRC, 165, 219, doi:10.1198/jasa.2007, 2005.

575 Gallagher, K.: Evolving temperature histories from apatite fission-track data, *Earth Planet Sci Lett*, 136, 3, 421-435, doi:10.1016/0012-821X(95)00197-K, 1995.

Gallagher, K.: Transdimensional inverse thermal history modeling for quantitative thermochronology, *J. Geophys. Res. Solid Earth*, 117, B2, <http://doi.wiley.com/10.1029/2011JB008825>, 2012.

580 Gleadow, A. J., Duddy, I. R., Green, P. F., and Hegarty, K. A.: Fission track lengths in the apatite annealing zone and the interpretation of mixed ages, *Earth Planet Sci Lett*, 78, 2-3, 245-254, doi:10.1016/0012-821X(86)90065-8, 1986a.

Gleadow, A. J. W., Duddy, I. R., Green, P. F., and Lovering, J. F.: Confined fission track lengths in apatite: a diagnostic tool for thermal history analysis, *Contrib Mineral Petr*, 94, 4, 405-415, doi:10.1007/BF00376334, 1986b.

585

Gleadow A., Kohn B., and Seiler C.: The Future of Fission-Track Thermochronology, in: *Fission-Track Thermochronology and its Application to Geology*, edited by Malusà M. and Fitzgerald P., Springer Textbooks in Earth Sciences, Geography and Environment, Springer, Cham, doi:10.1007/978-3-319-89421-8\_4, 2019.

590 Green, P. F., Duddy, I. R., Gleadow, A. J. W., Tingate, P. R., and Laslett, G. M.: Thermal annealing of fission tracks in apatite: I. A qualitative description, *Chem. Geol.: Isotope Geoscience section*, 59, 237-253, doi:10.1016/0168-9622(86)90074-6, 1986.

Green, P. F.: The relationship between track shortening and fission track age reduction in apatite: combined influences of inherent instability, annealing anisotropy, length bias and system calibration, *Earth Planet Sci Lett*, 89, 3-4, 335-352, doi:10.1016/0012-821X(88)90121-5, 1988.

595

Green, P. F., Duddy, I. R., Laslett, G. M., Hegarty, K. A., Gleadow, A. J. W., and Lovering, J. F., Thermal annealing of fission tracks in apatite 4. Quantitative modelling techniques and extension to geological timescales, *Chem. Geol.: Isotope Geoscience section*, 79, 2, 155-182, [https://doi.org/10.1016/0168-9622\(89\)90018-3](https://doi.org/10.1016/0168-9622(89)90018-3), 1989.

600

Hansen, K.: Thermotectonic evolution of a rifted continental margin: fission track evidence from the Kangerlussuaq area, SE Greenland, *Terra Nova*, 8, 5, 458-469, <http://doi.wiley.com/10.1111/j.1365-3121.1996.tb00771.x>, 1996.

605 Hansen, K., Bergman, S. C., and Henk, B.: The Jameson Land basin (east Greenland): a fission track study of the tectonic and thermal evolution in the Cenozoic North Atlantic spreading regime, *Tectonophysics*, 331, 3, 307-339, doi:10.1016/S0040-1951(00)00285-7, 2001.

Jensen, P. K., Hansen, K., and Kunzendorf, H.: A numerical model for the thermal history of rocks based on confined horizontal fission tracks. *International Journal of Radiation Applications and Instrumentation, Part D. Nucl. Tracks Radiat. Meas.*, 20, 2, 610 349-359, doi: 10.1016/1359-0189(92)90064-3, 1992.

Jensen, P. K., Bidstrup, T., Hansen, K., and Kunzendorf, H.: The Use of Fission Track Measurements in Basin Modeling, in: *Computerized Basin Analysis*, edited by: Harff, J. and Merriam, D. F., Springer US, doi:10.1007/978-1-4615-2826-5\_7, 1993.

615 Jensen, P. K. and Hansen, K.: Identifying the post-sedimentary part of fission track length histograms with inherited tracks, *Thermo 2018*, 16th International Conference on Thermochronology, Quedlinburg, Germany; 16-21 September 2018, <https://doi.org/10.1002/essoar.10500031.1>, 2018.

Jensen, P.K.: ~~Deconvolution of 2D- fission track length histograms~~~~Age versus length of horizontal fission tracks represented by 2D- Histograms~~, Zenodo, <https://doi.org/10.5281/zenodo.5137192>~~<https://doi.org/10.5281/zenodo.4553144>~~, 2021a.

Jensen, P.K.: ~~Deconvolution of 3D-fission track length histograms~~~~Age versus length of horizontal fission tracks represented by 3D- Histograms~~, Zenodo, <https://doi.org/10.5281/zenodo.5137293>~~<https://doi.org/10.5281/zenodo.4553291>~~, 2021b.

625 Jungerman, J. and Wright, S. C.: Kinetic Energy Release in Fission of U238, U235, Th232, and Bi209 by High Energy Neutrons, *Phys. Rev.*, 76, 1112-1116, doi:10.1103/PhysRev.76.1112 , 1949.

Keil, R., Pahl, M., and Bertagnolli, E.: Thermal history and length distribution of fission tracks: Part II, *International Journal of Radiation Applications and Instrumentation, Part D. Nucl. Tracks Radiat. Meas.*, 13, 1, 25-33, 1987.

630 Ketcham, R. A.: Observations on the relationship between crystallographic orientation and biasing in apatite fission-track measurements, *Am Min*, 88, 5-6, 817-829, 2003.

Ketcham, R. A.: Forward and inverse modeling of low-temperature thermochronometry data, *Rev Mineral and Geochem*, 58, 635 1, 275-314, doi:10.2138/am-2003-5-610, 2005.

Ketcham, R. A., Donelick, R. A., Balestrieri, M. L., and Zattin, M.: Reproducibility of apatite fission-track length data and thermal history reconstruction, *Earth Planet Sci Lett*, 284, 3-4, 504-515, 2009.

640 Ketcham R.A.: Fission-Track Annealing: From Geologic Observations to Thermal History Modeling, in: *Fission-Track Thermochronology and its Application to Geology*, edited by: Malusà M. and Fitzgerald P, Springer Textbooks in Earth Sciences, Geography and Environment, Springer, Cham., [https://doi.org/10.1007/978-3-319-89421-8\\_3](https://doi.org/10.1007/978-3-319-89421-8_3), 2019.

Kirkpatrick, S., Gelatt, C. D., and Vecchi, M. P.: Optimization by simulated annealing, *Science*, 220, 4598, 671-680, 1983.

645

Laslett, G. M., Gleadow, A. J. W., and Duddy, I. R.: The relationship between fission track length and track density in apatite, *Nucl. Tracks Radiat. Meas.*, (1982), 9, 1, 29-38, doi:10.1016/0735-245X(84)90019-X, 1984.

650 Li, W., Wang, L., Lang, M., Trautmann, C., and Ewing, R. C.: Thermal annealing mechanisms of latent fission tracks: Apatite vs. zircon, *Earth Planet Sci Lett*, 302, 1, 227-235, doi:10.1016/j.epsl.2010.12.016, 2011.

Lutz, T. M. and Omar, G.: An inverse method of modeling thermal histories from apatite fission-track data, *Earth Planet Sci Lett*, 104, 2-4, 181-195, doi:10.1016/0012-821X(91)90203-T 1991.

655 [Stephenson, J., Gallagher, K., and Holmes, C.: A Bayesian approach to calibrating apatite fission track annealing models for laboratory and geological timescales, \*Geochimica et Cosmochimica Acta\*, Volume 70, Issue 20, 5183-5200, 2006, https://doi.org/10.1016/j.gca.2006.07.027.](https://doi.org/10.1016/j.gca.2006.07.027)

Tarantola, A.: *Inverse problem theory*, SIAM, Philadelphia, doi:0.1137/1.9780898717921, 2005.

660

Willett, S. D.: Inverse modeling of annealing of fission tracks in apatite; 1, A controlled random search method, *Am. J. Sci.*, 297, 10, 939-969, doi:10.2475/ajs.297.10.939, 1997.